Environmental Science & Technology

pubs.acs.org/est

Article

Key Role of Equilibrium HONO Concentration over Soil in Quantifying Soil−Atmosphere HONO Fluxes

Fengxia Bao, Yafang Cheng, Uwe Kuhn, Guo Li, Wenjie Wang, Alexandra Maria Kratz, Jens Weber, Bettina Weber, Ulrich Pöschl, and Hang Su*

Cite This: *Environ. Sci. Technol.* 2022, 56, 2204−2212

Read Online

ACCESS | Metrics & More | Article Recommendations | Supporting Information

ABSTRACT: Nitrous acid (HONO) is an important component of the global nitrogen cycle and can regulate the atmospheric oxidative capacity. Soil is an important source of HONO. [HONO]*, the equilibrium gas-phase concentration over the aqueous solution of nitrous acid in the soil, has been suggested as a key parameter for quantifying soil fluxes of HONO. However, [HONO]* has not yet been well-validated and quantified. Here, we present a method to retrieve [HONO]* by conducting controlled dynamic chamber experiments with soil samples applied with different HONO concentrations at the chamber inlet. We show a bi-directional soil−atmosphere exchange of HONO and confirm the existence of [HONO]* over soil: when [HONO]* is higher than the atmospheric HONO concentration, HONO will be released from soil; otherwise, HONO will be deposited. We demonstrate that [HONO]* is a soil characteristic, which is independent of HONO concentrations in the chamber but varies with different soil water contents. We illustrate the robustness of using [HONO]* for quantifying soil fluxes of HONO, whereas the laboratory-determined chamber HONO fluxes can largely deviate from those in the real world for the same soil sample. This work advances the understanding of the soil−atmosphere exchange of HONO and the evaluation of its impact on the atmospheric oxidizing capacity.

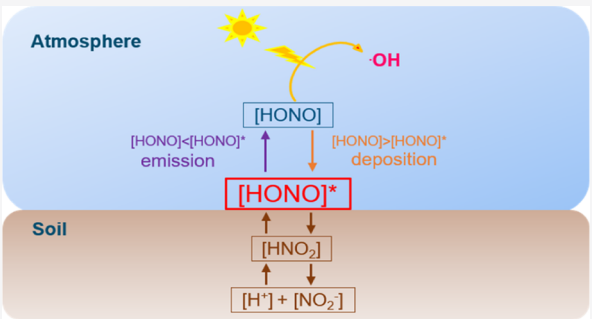

KEYWORDS: *HONO, equilibrium HONO concentration ([HONO]*), soil, nitrogen cycling, flux*

INTRODUCTION

Hydroxyl radicals (OH) are key species in maintaining photo-oxidation cycles in the atmosphere.[1] Gaseous nitrous acid (HONO) can be rapidly photolyzed under sunlight to produce OH radicals.[1−4] In polluted regions, the contribution of HONO to atmospheric OH radical concentrations has been reported to be comparable to or even greater than the contribution of other primary OH sources, for example, the photolysis of ozone and the ozonolysis of alkenes.[5−9]

The main source of atmospheric HONO has been a mystery for decades. Emission from combustion processes[10,11] and gas-phase production of HONO (via the reaction of NO with OH[12,13]) are not sufficient to explain the observed high atmospheric HONO concentrations in field studies.[14−17] A heterogeneous reaction of NO_2 on aerosol surfaces[14,18] has been suggested to explain the high HONO concentrations.[15,19] In the presence of light, the reaction has been observed to be significantly enhanced and has been considered to be a missing daytime HONO source.[20,21] However, the significance of such a source involving NO_2 uptake on aerosols remains controversial. Under atmospherically relevant conditions, the uptake coefficient of NO_2 (γ) on aerosols such as mineral dust,[22,23] soot,[20] and organic particulates[21] is at magnitudes of $<10^{-6}$, while γ of $>10^{-4}$ to 10^{-5} is required to explain the observed HONO formation rates of 0.2−2.0 ppb h^{-1}.[1,24−27] Additional HONO formation mechanism such as the photosensitized reduction of NO_2 on humic acid surfaces has been proposed.[2,28] Moreover, laboratory studies found that heterogeneous HNO_3 photolysis on aerosols exhibited a high HONO production rate and has been accounted as an important HONO source.[29−31] However, multiple scattering effects of light on aerosol sample filters used in those experiments may lead to an overestimation of the observed reaction rates.[32,33]

Besides chemical reactions, Su et al. showed that biogenic soil nitrite can be an important HONO source.[1] After production from nitrification and denitrification, soil nitrite actively participates in the reversible acid−base reaction [NO_2^- (aq) + H^+ (aq) ⇔ HNO_2 (aq)] and releases HONO to the atmosphere through liquid−gas partitioning [HNO_2 (aq) ⇔ HONO (g)]. Recently, several more studies have been

Received: October 4, 2021
Revised: December 22, 2021
Accepted: January 4, 2022
Published: February 1, 2022

https://doi.org/10.1021/acs.est.1c06716
Environ. Sci. Technol. 2022, 56, 2204−2212

conducted examining soil HONO fluxes[34−42] and the laboratory chamber fluxes were directly used as estimates of fluxes in the real world.[36,40−42] One problem of this treatment is the different transfer/deposition velocities of HONO in the laboratory and real-world conditions, which will lead to different fluxes under these two conditions. Up to now, there has been a lack of knowledge on how to translate measured fluxes in the laboratory chamber to those in the real world. In addition, most laboratory measurements have focused on measuring only HONO emission from soil by applying HONO-free air at the chamber inlet.[34,36,39,40] However, HONO deposition to soil should also be taken into account as it can occur at high atmospheric HONO concentrations. Micrometeorological field measurement methods of HONO fluxes, such as eddy correlation (EC), have been developed to directly determine HONO fluxes in the field.[37,43−45] However, it is still problematic due to the lack of rapid and sensitive techniques to measure HONO fluxes.[44] Empirical parameterization and process-based modeling is a labor-efficient alternative and several models have been used to simulate soil HONO fluxes.[34,46−50] Empirical parameterization models have calculated HONO emissions based on laboratory-determined chamber HONO fluxes as a function of soil water content (SWC).[34,46,51] A different approach has been suggested by Su et al.[1] based on the resistance model,[52−54] as shown in eq 1.

$$F = -v_t \times ([\mathrm{HONO}]_{atm} - [\mathrm{HONO}]^*) \quad (1)$$

where [HONO]* is the equilibrium gas-phase concentration over the aqueous solution of nitrous acid [HNO_2 (aq)] in the soil, $[\mathrm{HONO}]_{atm}$ is the atmospheric HONO concentration, and v_t represents the transfer/deposition velocity of HONO. The resistance model approach, being analogous to electrical current resistance,[54] accounts for three major processes that limit the transport of HONO from/to soil surfaces including (i) turbulent transport between the atmosphere and the top of the so-called quasi-laminar layer, a very thin layer of stagnant air adjacent to the soil surface, (ii) molecular transport across the quasi-laminar layer, and (iii) emission or deposition from/to the soil surface. Accordingly, three resistances in series, that is, the aerodynamic resistance R_a, the quasi-laminar layer resistance R_b, and the surface resistance R_c govern the HONO transport (see Figure S1).[1,55] v_t equals to the reciprocal of the total resistance (sum of R_a, R_b, and R_c). A major difference between eq 1 and other empirical parameterization methods is that it assumes the existence of [HONO]* and accounts for the effects of transfer/deposition velocities and atmospheric HONO concentrations.[1] If [HONO]*, as a soil characteristic, indeed exists, we argue that eq 1 is a reliable way to evaluate atmospheric HONO fluxes of soil. However, [HONO]* has not yet been validated and quantified experimentally.

In this study, we aim to demonstrate the existence of [HONO]* over soil, develop a method to derive [HONO]* by controlled dynamic chamber measurements, and quantify the atmospheric soil HONO fluxes. Moreover, [HONO]* variabilities during soil drying processes are investigated.

METHODS

Sampling. Soil samples were collected on 03 Aug 2020 from an agricultural wheat field in Mainz, Germany (49°59′33.7″N 8°13′05.5″E), at a depth of 0−5 cm. The collected samples were air-dried, grinded, and sieved through a 2 mm cutoff stainless-steel sieve and stored in the dark at room temperature for 3 months before analysis. The physicochemical properties of the soil sample are shown in Table S1.

Trace Gas-Exchange Measurements. The soil sample was prepared in a Petri glass dish (100 × 20 mm, Duran Group, Germany) containing 50 g of soil and 25 g of pure water (18.2 MΩ). The sample was thoroughly mixed by mechanical stirring and placed in dry purified air at room temperature to reach an SWC of 0.12 kg kg^{-1}, corresponding to 31% water holding capacity (WHC) of the soil. The sample was then placed into a dynamic flow-through chamber. The chamber had an inner diameter of 12.0 cm and a height of 13.0 cm. The inner wall material of the chamber was a 50 μm thin transparent Teflon film (FEP) (Saint Gobain Performance Plastics Corporation, USA). To control the temperature of the soil sample, the inner volume of the chamber bottom plate (made of PVDF) was continuously flushed with water cycled using a thermostat (Thermo Fisher Scientific, model SC100). The chamber was purged with purified air derived by passing ambient air through an ozone generator to oxidize nitrogen-containing trace gases, followed by sequential filter columns filled with glass wool (Merck, Germany), silica gel (2−5 mm, Merck, Germany), Purafil ($KMnO_4/Al_2O_3$, Purafil Inc. USA), and activated charcoal (LS—labor service, Germany). The inlet purging air was humidified using a PID-controlled split (dry/wet) gas system comprising two mass flow controllers (Bronkhorst High-Tech, Netherland) and RH sensors (KFS 140-TO, ±3% accuracy). Downstream of the humidification step, HONO gas was added to the inlet purging air at a small flow rate of 0.02−0.04 mL min^{-1} controlled using another mass flow controller. Many methods have been used to generate stable HONO.[56] Here, HONO gas was generated by flushing purified air through the headspace of a HONO source solution, which was prepared by dissolving $NaNO_2$ (1.25 mM) in a citric acid buffer (pH = 4) solution. The change in the HONO source concentration was less than 0.1 ppb within ∼10 h (Figure S2). From a total airflow of 6.9 L min^{-1}, only a fraction of 2.6 L min^{-1} was used to purge the chamber, as this amount was consumed using three gas analyzers. In the overflow exhaust pipe upstream of the chamber, a needle valve was installed. This variable flow resistance was used to keep the inner chamber volume at a slightly higher pressure than ambient, to prevent the risk of laboratory air contaminating the chamber. A Teflon-coated fan was installed in the center of the chamber lid to sustain highly turbulent conditions within the chamber.

HONO was measured with a commercial long path absorption photometer (LOPAP, QUMA, model LOPAP-03, Wuppertal, Germany). The estimated uncertainty of HONO measured by LOPAP is ∼10%. The lower detection limit was calculated from two times the standard deviation of the zero air signal (2σ) at ∼40 ppt for 1 min averages. The LOPAP technique is explained in detail elsewhere.[57] The gas-phase H_2O concentration was measured using an infrared CO_2/H_2O analyzer operated in the differential mode (LI-7000 LI-COR Biosciences GmbH, Bad Homburg, Germany). The variation of SWC was calculated using the measured differential water vapor concentrations between the chamber inlet and outlet at a given time (D_{Licor}) and the difference of the mass of the soil ($m_{soil,t=0}$) prior to and after ($m_{soil,t=N}$) the HONO exchange experiment

https://doi.org/10.1021/acs.est.1c06716
Environ. Sci. Technol. 2022, 56, 2204−2212

$$m_{\mathrm{soil},t=n} = m_{\mathrm{soil},t=0} - (m_{\mathrm{soil},t=0} - m_{\mathrm{soil},t=N}) \frac{\sum_{t=0}^{t=n} D_{\mathrm{Licor}}}{\sum_{t=0}^{t=N} D_{\mathrm{Licor}}} \quad (2)$$

$$\mathrm{SWC} = \frac{m_{\mathrm{soil},t=n} - m_{\mathrm{soil},d}}{m_{\mathrm{soil},d}} \quad (3)$$

Here, $t = 0$ denotes the time when the measurement started, $t = N$ is the time when the soil dried out, and $t = n$ is any time between $t = 0$ and N. $m_{\mathrm{soil,d}}$ is the mass of the oven-dried soil, which was determined by putting the soil sample in an oven at 110 °C for 24 h after the HONO exchange experiment. The wall loss of H_2O and HONO was corrected according to a reference measurement when the chamber was empty. The flow chart of the chamber system is shown in Figure S3.

[HONO]* Method. In the dynamic flow-through chamber, continuous purging air enters the chamber at the inlet, purges the chamber at a flow rate of Q, and exits the chamber at the outlet. The HONO flux (F) of soil is related to the transfer/deposition velocity (v_t) of HONO and the gradient between the HONO concentration of the chamber bulk headspace air (C_{cham}) and the equilibrium HONO concentration over the soil surface, [HONO]*,[1] here defined as C^*

$$F = -v_t \times (C_{\mathrm{cham}} - C^*) \quad (4)$$

To be noted, under ideal conditions, when the equilibrium in the soil is reached, [HONO]* over the soil surface would be the same as that in the soil. In practice, the equilibrium is expected to be reached within a shallow topsoil layer.

The HONO flux (F) can also be quantified using the chamber mass balance equation[58]

$$F = (C_{\mathrm{out}} - C_{\mathrm{in}}) \times \frac{Q}{A} + \frac{\mathrm{d}C_{\mathrm{cham}}}{\mathrm{d}t} \times \frac{V}{A} = \frac{V}{A \times \tau_{\mathrm{cham}}} \times ((C_{\mathrm{out}} - C_{\mathrm{in}}) + \frac{\mathrm{d}C_{\mathrm{cham}}}{\mathrm{d}t} \times \tau_{\mathrm{cham}}) \quad (5)$$

Here, V is the chamber volume and A denotes the soil surface area, C_{in} and C_{out} are the HONO concentrations measured at the chamber inlet and outlet, respectively, τ_{cham} is the residence time ($\tau_{\mathrm{cham}} = \frac{V}{Q}$) of the air within the chamber volume, and t is the experiment time. During the experiment, HONO concentrations at the chamber inlet were switched between three concentrations at time intervals of 15 min. The measured HONO concentrations from only minute 11 to 13 of each time interval were used to calculate [HONO]*. $\frac{\mathrm{d}C_{\mathrm{cham}}}{\mathrm{d}t} \times \tau_{\mathrm{cham}}$ in this time duration was negligible (0.02 ± 0.23 ppb), compared to C_{cham} (13.9 ± 8.13 ppb). Therefore, eq 5 can be reduced to

$$F \approx (C_{\mathrm{out}} - C_{\mathrm{in}}) \times \frac{Q}{A} \quad (6)$$

To be noted, eq 6 is only valid for calculating the flux of an inert trace gas, which shows no reactions with other air components in the chamber. HONO is chemically reactive under UV light. Since this study was conducted in the dark, HONO was considered inert. In addition, HONO concentration of the chamber headspace (C_{cham}) can be assumed uniform as the chamber air was well-mixed and hence also equals to the concentration measured at the chamber outlet (C_{out})

$$C_{\mathrm{cham}} = C_{\mathrm{out}} \quad (7)$$

Combining eqs 4, 6, and 7 gives

$$\frac{C^* - C_{\mathrm{out}}}{C_{\mathrm{out}} - C_{\mathrm{in}}} = \frac{Q}{A \times v_t} \quad (8)$$

When applying C_{in1} of HONO concentration at the chamber inlet and measuring the concentration at the chamber outlet (C_{out1}), the following equation is obtained

$$\frac{C^* - C_{\mathrm{out1}}}{C_{\mathrm{out1}} - C_{\mathrm{in1}}} = \frac{Q}{A \times v_t} \quad (9)$$

When HONO concentration at the chamber inlet was switched to C_{in2}, the concentration at the chamber outlet (C_{out2}) was measured. A similar equation as eq 9 is obtained

$$\frac{C^* - C_{\mathrm{out2}}}{C_{\mathrm{out2}} - C_{\mathrm{in2}}} = \frac{Q}{A \times v_t} \quad (10)$$

Here, soil conditions during C_{out2} were the same as during the determination of C_{out1} (see Figure S4 for details), and thus, parameters on the right-hand side of eqs 9 and 10 are the same and can be combined as

$$\frac{C^* - C_{\mathrm{out1}}}{C_{\mathrm{out1}} - C_{\mathrm{in1}}} = \frac{C^* - C_{\mathrm{out2}}}{C_{\mathrm{out2}} - C_{\mathrm{in2}}} \quad (11)$$

In this way, the unknown parameters (A and v_t) are canceled out and C^* can be solved from eq 11

$$C^* = \frac{C_{\mathrm{in1}} \times C_{\mathrm{in2}} - C_{\mathrm{in2}} \times C_{\mathrm{out1}}}{C_{\mathrm{in1}} - C_{\mathrm{in2}} + C_{\mathrm{out2}} - C_{\mathrm{out1}}} \quad (12)$$

The method is applicable to obtain equilibrium concentrations not only of HONO but also of other trace gases over soil and other surfaces. Because the equilibrium relative humidity (RH*) of air over a liquid water surface is known to be 100%, a chamber test with liquid water in a Petri dish was performed to validate the applicability of the abovedescribed C^* method by comparing the observation-based RH* with the theoretically assumed 100% (see the Supporting Information for details). The RH* results showed no dependence on different chamber turbulent conditions (Figure S5 and Table S2) and the mean of the RH* results of all tests was 97.4%. The consistency of mean RH* under different chamber turbulent conditions and the proximity of the RH* to 100% confirm the validity of the C^* method, that is, retrieving C^* from a set of two different inlet concentrations while monitoring the respective outlet concentrations.

RESULTS AND DISCUSSION

HONO Exchange of Soil at Different Inlet HONO Concentrations. Figure 1 shows the results of a HONO exchange experiment of a soil sample. The SWC gradually decreased during the experiment as semihumidified air (46% RH) was applied. Inlet HONO concentrations were sequentially switched between three different concentrations (0, 5, and 15 ppb) in 15 min intervals. For all three inlet HONO concentrations, the HONO concentration at the chamber outlet exhibited a similar trend with respect to the decreasing SWC. Observed outlet HONO concentrations first increased as the SWC decreased. After reaching a maximum at an SWC of 0.04 kg kg^{-1} (10% WHC), the HONO concentrations decreased. This pattern of soil HONO emission

https://doi.org/10.1021/acs.est.1c06716
Environ. Sci. Technol. 2022, 56, 2204−2212

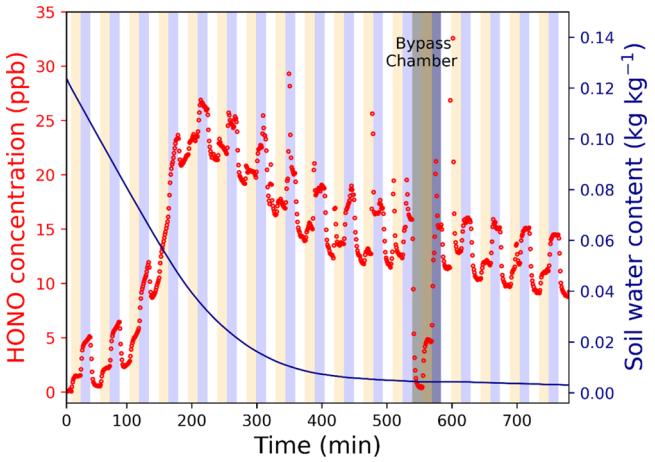

Figure 1. Change in HONO concentration at the chamber outlet (left, red) and SWC (right, dark blue) over time of the soil drying process when the HONO concentration of the inlet purging air was switched between 0 ppb (white-shaded), 5 ppb (yellow-shaded), and 15 ppb (blue-shaded) in 15 min intervals. The grey-shaded area indicates when the inlet purging air bypassed the chamber to check the stability of the inlet HONO concentrations.

during the soil drying process is similar to that found in previous studies.[1,36]

To see the influence of inlet HONO concentrations on the soil HONO fluxes, the outlet HONO concentration data were evaluated independently from each other according to the three inlet HONO concentrations applied (Figure 2). At an inlet HONO concentration of 0 ppb, net emission of HONO persisted throughout the whole soil drying process. At 5 and 15 ppb of HONO applied at the inlet, the outlet HONO concentration was first found lower than the inlet HONO concentration, indicating net HONO deposition to the soil. As the SWC continued to decrease, net HONO emission was observed. These results show that either HONO emission from or deposition to soil occurs at different inlet HONO concentrations. Different inlet HONO concentrations cause different HONO concentrations in the chamber headspace, which correspond to atmospheric concentrations of HONO in the real world. These results suggest that whether HONO is emitted from or deposited to soil depends not only on soil properties but also on atmospheric HONO concentrations, contributed by different HONO sources and sinks.

[HONO]*, the equilibrium gas-phase HONO concentration over the soil, has been suggested to be an important parameter to determine the bi-directional HONO exchange between soil and the atmosphere.[1] Up to now, only theoretical [HONO]* values have been calculated according to pH and nitrite content of bulk soils.[1,59] In this work, we introduced a method to retrieve the actual [HONO]* values during the soil drying process (see the Methods for details). To check for consistency, two different result combinations of applied inlet HONO concentrations were used to calculate [HONO]* according to eq 12, that is, grouping 0 and 15 ppb ($[HONO]^*_1$) and grouping 5 and 15 ppb ($[HONO]^*_2$). As shown in Figure 3, there was a close correlation between $[HONO]^*_1$ and $[HONO]^*_2$. These results show that the retrieved [HONO]* is independent of the inlet HONO concentrations applied, which proves that [HONO]* indeed exists as a soil characteristic. As shown in Figure 2, [HONO]* regulates both the direction and the magnitude of HONO exchanges from/to the soil. When [HONO]* is higher than the HONO concentration of the chamber headspace air ($[HONO]_{out}$), HONO will be released from the soil; otherwise, HONO will be deposited to the soil. In the real world, the comparison between [HONO]* and atmospheric HONO concentrations can predict whether HONO is emitted from or deposited to the soil. Furthermore, [HONO]* is strongly dependent on SWC as shown in Figure 4. As the SWC decreased, [HONO]* increased to a maximum (~31 ppb) at an SWC of 0.04 kg kg^{-1} (10% WHC) and then [HONO]* decreased as SWC further decreased. When SWC decreases, the increasing concentration of HNO_2 (aq) in soil water can lead to a higher [HONO]*, according to Henry's law behavior of gas−liquid partitioning [HNO_2 (aq) ⇔ HONO (g)]. This, however, could not explain the decrease in [HONO]* when SWC further decreases. A possible explanation is the limited kinetic mass transport and the nonideal solution behavior at lower SWC.[60]

Quantification of Soil HONO Fluxes. The chamber HONO flux from/to the soil sample was calculated according to eq 6. At the three inlet HONO concentrations, the chamber HONO fluxes ranged from −31.1 to 68.6 ng N m^{-2} s^{-1} at different SWCs during the soil drying process (Figure 5A). In previous studies, HONO fluxes of soil derived from dynamic chamber measurements have been adopted directly to predict fluxes in the real world.[36,40−42] However, fluxes determined in the laboratory chamber can vary greatly from fluxes in the real world, mainly due to the different transfer/deposition

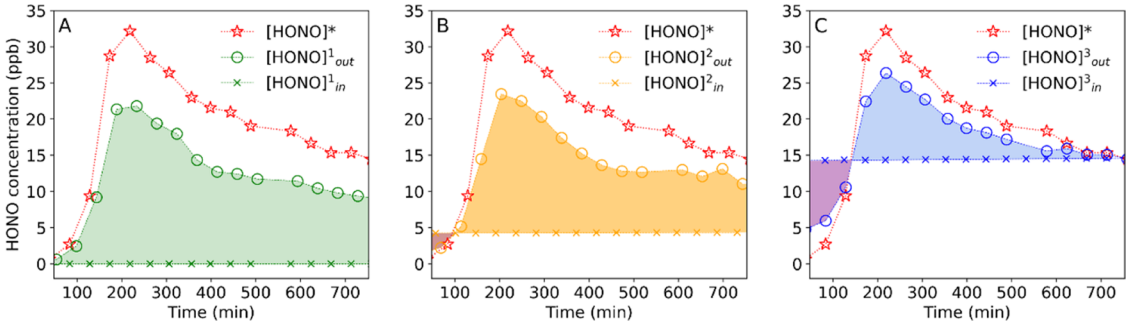

Figure 2. HONO concentration (O) at the chamber outlet when the inlet HONO concentration (X) was switched between 0 (A), 5 (B), and 15 ppb (C) and the equilibrium HONO concentration ([HONO]* (☆), the mean of $[HONO]^*_1$ and $[HONO]^*_2$, see Figure 3) over time of the soil drying process. Color-shaded areas indicate periods of emission (light color) or deposition (dark color), respectively. Note that Figure 2 was obtained by separating the data in Figure 1 according to the three inlet HONO concentrations applied.

https://doi.org/10.1021/acs.est.1c06716
Environ. Sci. Technol. 2022, 56, 2204−2212

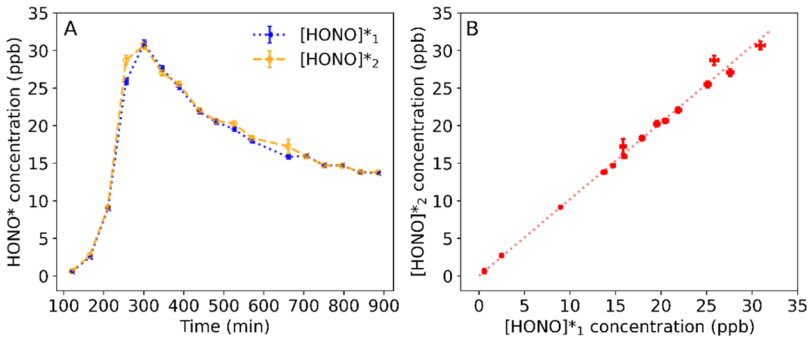

Figure 3. Equilibrium HONO concentrations, $[HONO]^*_1$ (blue) and $[HONO]^*_2$ (orange) over time of the soil drying process (A) and their correlation with each other (B). The red dotted line represents the linear fit on the data points (slope = 1.02, R^2 = 1.00). $[HONO]^*_1$, $[HONO]^*_2$, and $[HONO]^*_3$ (Figure S6) were calculated based on three different result combinations of the applied inlet HONO concentrations, that is, grouping 0 ppb and 15 ppb, grouping 5 and 15 ppb, and grouping 0 and 5 ppb, respectively. Error bars indicate the uncertainties in the [HONO]* retrieval, estimated by the Monte Carlo method (see details in Figure S6). Note that the uncertainty of $[HONO]^*_3$ was large with an average of ±1.02 ppb, compared to that of $[HONO]^*_1$ (±0.27 ppb) and $[HONO]^*_2$ (±0.34 ppb). Therefore, $[HONO]^*_3$ was not included here for comparison.

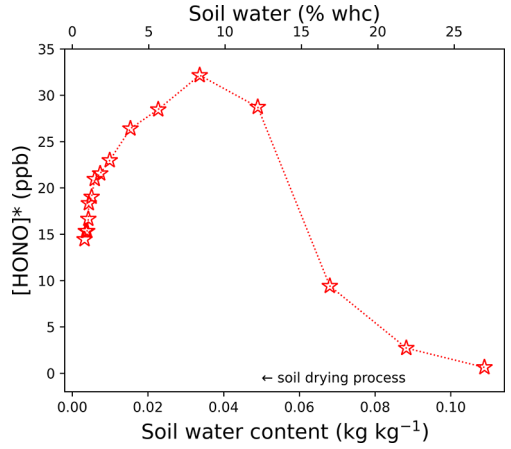

Figure 4. Equilibrium HONO concentrations [HONO]* (mean of $[HONO]^*_1$ and $[HONO]^*_2$) at different SWCs during the soil drying process.

velocities under laboratory conditions and real-world conditions. We show this by examining chamber H_2O vapor fluxes of pure liquid water as a well-controllable proxy for fluxes of trace gas species (Figure S7). Chamber H_2O vapor fluxes were observed to be strongly dependent on chamber turbulent conditions. On the other hand, as noted above in the [HONO]* method section, the turbulent conditions did not significantly affect the observation-based RH* (Figure S5), which indirectly demonstrates the robustness of the [HONO]* method.

[HONO]* is a soil characteristic and does not depend on chamber mixing levels or purging flow rates, thus being better suited to estimate HONO fluxes in the real world. Soils from different environments can be collected and [HONO]* can be retrieved by the described [HONO]* method. In addition to [HONO]*, the transfer/deposition velocity (v_t) and the atmospheric concentration of HONO ($[HONO]_{atm}$) are also crucial parameters for quantifying soil HONO fluxes according to eq 1. v_t depends primarily on the meteorological conditions and soil resistances, and the reported v_t values fall in the range of 0.077−3 cm s^{-1}.[61−65] Field observations of $[HONO]_{atm}$ have been extensively performed (Table S3) and up to ∼10 ppb of $[HONO]_{atm}$ have been reported for a fertilized agricultural field site in the North China Plain.[66] [HONO]* at different SWCs during the drying process of an agricultural soil sample was determined by the present study (Figure 4). Accordingly, the predicted atmospheric HONO fluxes range from −54.8 to 179.6 ng m^{-2} s^{-1} if adopting $[HONO]_{atm}$ of 0−10 ppb and a typical v_t of 1 cm s^{-1} (Figure 5B).[1] When

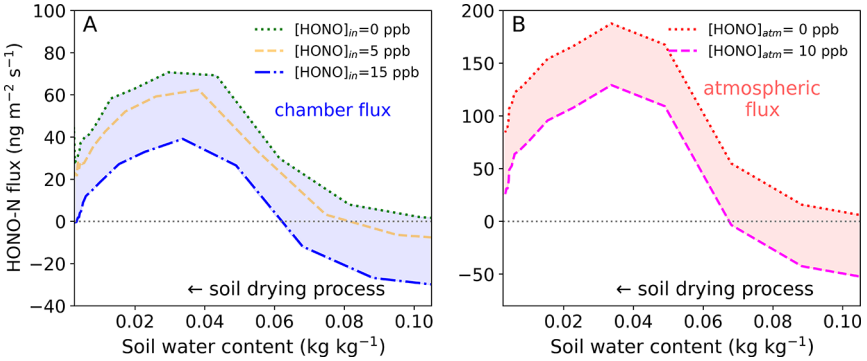

Figure 5. Chamber HONO fluxes (A) calculated by eq 6 on the basis of soil geometric surface area when inlet HONO concentrations were 0 ppb (···, green), 5 ppb (---, orange), and 15 ppb (-·-, blue) and atmospheric HONO fluxes (B) calculated by eq 1 using equilibrium HONO concentrations ([HONO]*) at different SWCs during the soil drying process retrieved by the [HONO]* method. Atmospheric HONO concentrations ($[HONO]_{atm}$) of 0 (···, pink) and 10 ppb (---, magenta), both with a HONO transfer/deposition velocity (v_t) of 1 cm s^{-1} were adopted for calculation.

https://doi.org/10.1021/acs.est.1c06716
Environ. Sci. Technol. 2022, 56, 2204−2212

adopting v_t of 0.077−3 cm s^{-1}, the predicted atmospheric HONO fluxes range from −164.5 (when $[HONO]_{atm}$ = 10 ppb) to 538.7 ng m^{-2} s^{-1} (when $[HONO]_{atm}$ = 0 ppb), as shown in Figure S8. These results show that the predicted atmospheric HONO fluxes can differ widely from HONO fluxes measured in the chamber (Figure 5A), which is due to different HONO concentrations and v_t in the chamber and in the real world. These results illustrate that the chamber-derived HONO fluxes cannot be directly used to estimate HONO fluxes of soil in the real world.

Meusel et al. estimated [HONO]* by a simplified method using measurements of the water−air exchange of H_2O vapor.[39] Assuming a similar concentration gradient between the chamber headspace air and the surfaces of soil and liquid water for HONO and H_2O vapor, [HONO]* can be estimated by

$$[HONO]^* \approx \frac{[H_2O]^* \times [HONO]_{out}}{[H_2O]_{out}} \quad (13)$$

where $[H_2O]^*$ is the known saturation water vapor concentration (100% RH), $[H_2O]_{out}$ is the measured H_2O concentration at the chamber outlet with inlet dry air, and $[HONO]_{out}$ is the measured HONO concentration at the chamber outlet at an inlet HONO concentration of 0 ppb. In Figure S9, [HONO]* derived by the $[H_2O]$ method shows a good agreement (within 30%) with that derived by the [HONO]* method of the present study. This suggests that the transfer/deposition velocities, v_t, of HONO and H_2O vapor are similar in the same chamber system. v_t equals to the reciprocal of the sum of R_a, R_b, and R_c (Figure S1). R_a, the aerodynamic resistance, is the same for surface−air exchange of these two species in the same chamber system. Smaller [HONO]* values derived by the $[H_2O]$ method than those by the [HONO]* method could be explained by the smaller R_b, quasi-laminar layer resistance, and R_c, surface resistance for the water−air exchange of H_2O vapor than those for soil−air exchange of HONO. For the [HONO]* method, two sets of HONO measurement results under the same soil and chamber conditions were used for [HONO]* calculation, which guaranteed that R_a, R_b, and R_c were all the same. [HONO]* can then be solved accurately.

As aforementioned, theoretical [HONO]* can be calculated from values of nitrite concentration and pH in soil water, along with temperature and SWC.[1] Assuming an SWC of 0.04 kg kg^{-1}, the theoretical [HONO]* of the soil sample at the experiment temperature (22 °C) was calculated to be ∼0.3 ppb according to its nitrite content (0.43 mg kg^{-1}) and pH (7.7) measured before the soil drying process. In comparison, the observation-based [HONO]* at an SWC of 0.04 kg kg^{-1} was ∼30.8 ppb (Figure 4). The deviations can be caused by a variable nitrite content during the soil drying process due to active N-transforming microorganisms.[67] In addition, the nitrite concentrations and pH across the soil can vary by orders of magnitude.[48] Besides the dynamics, surface layer soil or soil solution is also not an ideal solution, the nonideality and adsorption equilibrium may differ from the results based on an ideal solution system. Moreover, the kinetic limitation, for example, change in diffusion in soil water pores due to restricting of soil water in the course of drying, would also play a role in the change in HONO fluxes, which would further complicate the [HONO]* calculation. In contrast, the [HONO]* method in the present study determines an overall equilibrium concentration over the soil surface. Therefore, the observation-based [HONO]* values (Figure 4) are more atmospherically relevant in quantifying soil−atmosphere HONO fluxes.

Atmospheric Implication. The present study shows that the exchange of HONO between soil and the atmosphere is bidirectional and provides direct evidence of the [HONO]* existence over soil. This soil−atmosphere exchange of HONO is mainly regulated by [HONO]* and the atmospheric HONO concentration ($[HONO]_{atm}$). Both [HONO]* and $[HONO]_{atm}$ can be affected by various environmental factors. For example, high temperature during daytime leads to increased [HONO]* due to the temperature dependence of the equilibrium of HNO_2 dissociation and gas−liquid partitioning on the soil surface.[1] At the same time, the photolysis of HONO under sunlight causes a relatively low daytime $[HONO]_{atm}$. As a result, [HONO]* is larger than $[HONO]_{atm}$ during daytime and HONO emission from the soil should prevail. In this scenario, soil will be a daytime HONO source, which helps us to explain the missing HONO sources observed during daytime.[5,68] During nighttime, a decreased [HONO]* at low temperature and a relatively high $[HONO]_{atm}$ due to the absence of photolysis can lead to HONO deposition to the soil and soil will be a HONO sink. Therefore, such diurnal variations of temperature and sunlight could lead to diurnal patterns of HONO fluxes between soil and the atmosphere. Our predicted pattern is in accordance with the observed diurnal HONO fluxes in an agricultural field.[66] Besides temperature, other parameters can also influence [HONO]*, such as SWC, soil nitrite, pH, and microbial activity. Although there is an increasing body of field measurements of $[HONO]_{atm}$, experimental investigations and model simulations on [HONO]* are still required to unravel and quantify soil HONO fluxes under different environmental conditions. In addition, [HONO]* is also linked with soil moisture and chemical, physical, and biological processes in the soil. We recommend further studies to investigate the dependence of [HONO]* on HONO gas−liquid/gas−solid exchanges and the kinetic mass transport in the soil. It is also feasible to apply the [HONO]* method in the field to derive [HONO]* of soil with its original properties and thickness. Investigations of [HONO]* could improve our predictions of atmospheric HONO fluxes of soil and our understanding of how the biosphere affects air quality and global climate.

■ ASSOCIATED CONTENT

Supporting Information

The Supporting Information is available free of charge at https://pubs.acs.org/doi/10.1021/acs.est.1c06716.

Details of validation of the equilibrium relative humidity (RH*) over a pure liquid water surface, resistance model for HONO fluxes of soil, stability of inlet HONO concentrations, chamber system, interpolation of C_{out} for [HONO]* calculation, RH* measurements, HONO* uncertainty, chamber H_2O vapor fluxes under different chamber conditions, predicted atmospheric HONO fluxes when adopting different $[HONO]_{atm}$ and v_t, comparison of [HONO]* derived by two methods, soil physicochemical properties, RH* under different chamber turbulence conditions, and summarizing HONO measurements (PDF)

https://doi.org/10.1021/acs.est.1c06716
Environ. Sci. Technol. 2022, 56, 2204−2212

AUTHOR INFORMATION

Corresponding Author

Hang Su − *Multiphase Chemistry Department, Max Planck Institute for Chemistry, Mainz 55128, Germany;* orcid.org/0000-0003-4889-1669; Email: h.su@mpic.de

Authors

Fengxia Bao − *Multiphase Chemistry Department, Max Planck Institute for Chemistry, Mainz 55128, Germany;* orcid.org/0000-0002-0208-1620

Yafang Cheng − *Minerva Research Group, Max Planck Institute for Chemistry, Mainz 55128, Germany; Department of Precision Machinery and Precision Instrumentation, University of Science and Technology of China, Hefei 230026, China;* orcid.org/0000-0003-4912-9879

Uwe Kuhn − *Multiphase Chemistry Department, Max Planck Institute for Chemistry, Mainz 55128, Germany*

Guo Li − *Multiphase Chemistry Department, Max Planck Institute for Chemistry, Mainz 55128, Germany;* orcid.org/0000-0002-0350-9879

Wenjie Wang − *Multiphase Chemistry Department, Max Planck Institute for Chemistry, Mainz 55128, Germany*

Alexandra Maria Kratz − *Multiphase Chemistry Department, Max Planck Institute for Chemistry, Mainz 55128, Germany*

Jens Weber − *Institute of Biology, University of Graz, Graz 8010, Austria; Multiphase Chemistry Department, Max Planck Institute for Chemistry, Mainz 55128, Germany*

Bettina Weber − *Institute of Biology, University of Graz, Graz 8010, Austria; Multiphase Chemistry Department, Max Planck Institute for Chemistry, Mainz 55128, Germany;* orcid.org/0000-0002-5453-3967

Ulrich Pöschl − *Multiphase Chemistry Department, Max Planck Institute for Chemistry, Mainz 55128, Germany;* orcid.org/0000-0003-1412-3557

Complete contact information is available at: https://pubs.acs.org/10.1021/acs.est.1c06716

Funding

Open access funded by Max Planck Society.

Notes

The authors declare no competing financial interest.

ACKNOWLEDGMENTS

This work was supported by the Max Planck Society (MPG). G.L. acknowledges the financial support from the China Scholarship Council (CSC).

REFERENCES

(1) Su, H.; Cheng, Y.; Oswald, R.; Behrendt, T.; Trebs, I.; Meixner, F. X.; Andreae, M. O.; Cheng, P.; Zhang, Y.; Pöschl, U. Soil Nitrite as a Source of Atmospheric HONO and OH Radicals. *Science* **2011**, *333*, 1616−1618.

(2) Stemmler, K.; Ammann, M.; Donders, C.; Kleffmann, J.; George, C. Photosensitized Reduction of Nitrogen Dioxide on Humic Acid as a Source of Nitrous Acid. *Nature* **2006**, *440*, 195−198.

(3) Kleffmann, J.; Gavriloaiei, T.; Hofzumahaus, A.; Holland, F.; Koppmann, R.; Rupp, L.; Schlosser, E.; Siese, M.; Wahner, A. Daytime Formation of Nitrous Acid: A Major Source of OH Radicals in a Forest. *Geophys. Res. Lett.* **2005**, *32*, 1−4.

(4) Platt, U.; Perner, D.; Harris, G. W.; Winer, A. M.; Pitts, J. N. Observations of Nitrous Acid in an Urban Atmosphere by Differential Optical Absorption. *Nature* **1980**, *285*, 312−314.

(5) Xue, C.; Zhang, C.; Ye, C.; Liu, P.; Catoire, V.; Krysztofiak, G.; Chen, H.; Ren, Y.; Zhao, X.; Wang, J.; Zhang, F.; Zhang, C.; Zhang, J.; An, J.; Wang, T.; Chen, J.; Kleffmann, J.; Mellouki, A.; Mu, Y. HONO Budget and Its Role in Nitrate Formation in the Rural North China Plain. *Environ. Sci. Technol.* **2020**, *54*, 11048−11057.

(6) Tan, Z.; Fuchs, H.; Lu, K.; Hofzumahaus, A.; Bohn, B.; Broch, S.; Dong, H.; Gomm, S.; Häseler, R.; He, L.; Holland, F.; Li, X.; Liu, Y.; Lu, S.; Rohrer, F.; Shao, M.; Wang, B.; Wang, M.; Wu, Y.; Zeng, L.; Zhang, Y.; Wahner, A.; Zhang, Y. Radical Chemistry at a Rural Site (Wangdu) in the North China Plain: Observation and Model Calculations of OH, HO_2 and RO_2 Radicals. *Atmos. Chem. Phys.* **2017**, *17*, 663−690.

(7) Gomez Alvarez, E.; Amedro, D.; Afif, C.; Gligorovski, S.; Schoemaecker, C.; Fittschen, C.; Doussin, J.-F.; Wortham, H. Unexpectedly High Indoor Hydroxyl Radical Concentrations Associated with Nitrous Acid. *Proc. Natl. Acad. Sci. U.S.A.* **2013**, *110*, 13294−13299.

(8) Zhang, J.; Guo, Y.; Qu, Y.; Chen, Y.; Yu, R.; Xue, C.; Yang, R.; Zhang, Q.; Liu, X.; Mu, Y.; Wang, J.; Ye, C.; Zhao, H.; Sun, Q.; Wang, Z.; An, J. Effect of Potential HONO Sources on Peroxyacetyl Nitrate (PAN) Formation in Eastern China in Winter. *J. Environ. Sci.* **2020**, *94*, 81−87.

(9) Kim, S.; VandenBoer, T. C.; Young, C. J.; Riedel, T. P.; Thornton, J. A.; Swarthout, B.; Sive, B.; Lerner, B.; Gilman, J. B.; Warneke, C.; Roberts, J. M.; Guenther, A.; Wagner, N. L.; Dubé, W. P.; Williams, E.; Brown, S. S. The Primary and Recycling Sources of OH during the NACHTT-2011 Campaign: HONO as an Important OH Primary Source in the Wintertime. *J. Geophys. Res.: Atmos.* **2014**, *119*, 6886−6896.

(10) Keene, W. C.; Lobert, J. M.; Crutzen, P. J.; Maben, J. R.; Scharffe, D. H.; Landmann, T.; Hély, C.; Brain, C. Emissions of Major Gaseous and Particulate Species during Experimental Burns of Southern African Biomass. *J. Geophys. Res.: Atmos.* **2006**, *111*, D04301.

(11) Liu, Y.; Nie, W.; Xu, Z.; Wang, T.; Wang, R.; Li, Y.; Wang, L.; Chi, X.; Ding, A. Semi-Quantitative Understanding of Source Contribution to Nitrous Acid (HONO) Based on 1 Year of Continuous Observation at the SORPES Station in Eastern China. *Atmos. Chem. Phys.* **2019**, *19*, 13289−13308.

(12) You, A.; Be, M. A. Y.; In, I. Flash Photochemical Study of the Reaction OH +NO +M Using Resonance Fluorescent Detection of OH. *J. Chem. Phys.* **2003**, *57*, 3677−3679.

(13) Pagsberg, P.; Bjergbakke, E.; Ratajczak, E.; Sillesen, A. Kinetics of the Gas Phase Reaction OH + NO (+ M) HONO (+ M) and the Determination of the UV Absorption Cross Sections of HONO. *Chem. Phys. Lett.* **1997**, *272*, 383−390.

(14) Ammann, M.; Kalberer, M.; Jost, D. T.; Tobler, L.; Rössler, E.; Piguet, D.; Gäggeler, H. W.; Baltensperger, U. Heterogeneous Production of Nitrous Acid on Soot in Polluted Air Masses. *Nature* **1998**, *395*, 157−160.

(15) Su, H.; Cheng, Y. F.; Shao, M.; Gao, D. F.; Yu, Z. Y.; Zeng, L. M.; Slanina, J.; Zhang, Y. H.; Wiedensohler, A. Nitrous Acid (HONO) and Its Daytime Sources at a Rural Site during the 2004 PRIDE-PRD Experiment in China. *J. Geophys. Res.* **2008**, *113*, D14312.

(16) Yang, W.; You, D.; Li, C.; Han, C.; Tang, N.; Yang, H.; Xue, X. Photolysis of Nitroaromatic Compounds under Sunlight: A Possible Daytime Photochemical Source of Nitrous Acid? *Environ. Sci. Technol. Lett.* **2021**, *8*, 747.

(17) Spataro, F.; Ianniello, A.; Esposito, G.; Allegrini, I.; Zhu, T.; Hu, M. Occurrence of Atmospheric Nitrous Acid in the Urban Area of Beijing (China). *Sci. Total Environ.* **2013**, *447*, 210−224.

(18) Finlayson-Pitts, B. J.; Wingen, L. M.; Sumner, A. L.; Syomin, D.; Ramazan, K. A. The Heterogeneous Hydrolysis of NO2 in Laboratory Systems and in Outdoor and Indoor Atmospheres: An Integrated Mechanism. *Phys. Chem. Chem. Phys.* **2003**, *5*, 223−242.

(19) Kleffmann, J. Daytime Sources of Nitrous Acid (HONO) in the Atmospheric Boundary Layer. *ChemPhysChem* **2007**, *8*, 1137−1144.

(20) Monge, M. E.; D'Anna, B.; Mazri, L.; Giroir-Fendler, A.; Ammann, M.; Donaldson, D. J.; George, C. Light Changes the

Atmospheric Reactivity of Soot. *Proc. Natl. Acad. Sci. U.S.A.* **2010**, *107*, 6605−6609.
(21) Stemmler, K.; Ndour, M.; Elshorbany, Y.; Kleffmann, J.; D'Anna, B.; George, C.; Bohn, B.; Ammann, M. Light Induced Conversion of Nitrogen Dioxide into Nitrous Acid on Submicron Humic Acid Aerosol. *Atmos. Chem. Phys.* **2007**, *7*, 4237−4248.
(22) Ullerstam, M.; Johnson, M. S.; Vogt, R.; Ljungström, E. DRIFTS and Knudsen Cell Study of the Heterogeneous Reactivity of SO_3 and NO_2 on Mineral Dust. *Atmos. Chem. Phys.* **2003**, *3*, 2043−2051.
(23) Underwood, G. M.; Song, C. H.; Phadnis, M.; Carmichael, G. R.; Grassian, V. H. Heterogeneous Reactions of and HNO_3 on Oxides and Mineral Dust: A Combined Laboratory and Modeling Study. *J. Geophys. Res.* **2001**, *106*, 18055−18066.
(24) Zhou, X.; Gao, H.; He, Y.; Huang, G.; Bertman, S. B.; Civerolo, K.; Schwab, J. Nitric Acid Photolysis on Surfaces in Low-NOx Environments: Significant Atmospheric Implications. *Geophys. Res. Lett.* **2003**, *30*, 2217.
(25) Ren, X.; Harder, H.; Martinez, M.; Lesher, R. L.; Oliger, A.; Simpas, J. B.; Brune, W. H.; Schwab, J. J.; Demerjian, K. L.; He, Y.; Zhou, X.; Gao, H. OH and HO_2 Chemistry in the Urban Atmosphere of New York City. *Atmos. Environ.* **2003**, *37*, 3639−3651.
(26) Ren, X.; Brune, W. H.; Mao, J.; Mitchell, M. J.; Lesher, R. L.; Simpas, J. B.; Metcalf, A. R.; Schwab, J. J.; Cai, C.; Li, Y. Behavior of OH and HO_2 in the Winter Atmosphere in New York City. *Atmos. Environ.* **2006**, *40*, 252−263.
(27) Zhang, L.; Wang, T.; Zhang, Q.; Zheng, J.; Xu, Z.; Lv, M. Potential Sources of Nitrous Acid (HONO) and Their Impacts on Ozone: A WRF-Chem Study in a Polluted Subtropical Region. *J. Geophys. Res.: Atmos.* **2016**, *121*, 3645−3662.
(28) Han, C.; Yang, W.; Wu, Q.; Yang, H.; Xue, X. Heterogeneous Photochemical Conversion of NO_2 to HONO on the Humic Acid Surface under Simulated Sunlight. *Environ. Sci. Technol.* **2016**, *50*, 5017−5023.
(29) Bao, F.; Jiang, H.; Zhang, Y.; Li, M.; Ye, C.; Wang, W.; Ge, M.; Chen, C.; Zhao, J. The Key Role of Sulfate in the Photochemical Renoxification on Real PM2.5. *Environ. Sci. Technol.* **2020**, *54*, 3121−3128.
(30) Ye, C.; Zhang, N.; Gao, H.; Zhou, X. Photolysis of Particulate Nitrate as a Source of HONO and NOx. *Environ. Sci. Technol.* **2017**, *51*, 6849−6856.
(31) Bao, F.; Li, M.; Zhang, Y.; Chen, C.; Zhao, J. Photochemical Aging of Beijing Urban PM2.5: HONO Production. *Environ. Sci. Technol.* **2018**, *52*, 6309−6316.
(32) Su, H.; Cheng, Y.; Pöschl, U. New Multiphase Chemical Processes Influencing Atmospheric Aerosols, Air Quality, and Climate in the Anthropocene. *Acc. Chem. Res.* **2020**, *53*, 2034−2043.
(33) Bond, T. C.; Bergstrom, R. W. Light Absorption by Carbonaceous Particles: An Investigative Review. *Aerosol Sci. Technol.* **2006**, *40*, 27−67.
(34) Oswald, R.; Behrendt, T.; Ermel, M.; Wu, D.; Su, H.; Cheng, Y.; Breuninger, C.; Moravek, A.; Mougin, E.; Delon, C.; Loubet, B.; Pommerening-Röser, A.; Sörgel, M.; Pöschl, U.; Hoffmann, T.; Andreae, M. O.; Meixner, F. X.; Trebs, I. HONO Emissions from Soil Bacteria as a Major Source of Atmospheric Reactive Nitrogen. *Science* **2013**, *341*, 1233−1235.
(35) Donaldson, M. A.; Bish, D. L.; Raff, J. D. Soil Surface Acidity Plays a Determining Role in the Atmospheric-Terrestrial Exchange of Nitrous Acid. *Proc. Natl. Acad. Sci. U.S.A.* **2014**, *111*, 18472−18477.
(36) Weber, B.; Wu, D.; Tamm, A.; Ruckteschler, N.; Rodríguez-Caballero, E.; Steinkamp, J.; Meusel, H.; Elbert, W.; Behrendt, T.; Sörgel, M.; Cheng, Y.; Crutzen, P. J.; Su, H.; Pöschl, U.; Wofsy, S. C. Biological Soil Crusts Accelerate the Nitrogen Cycle through Large NO and HONO Emissions in Drylands. *Proc. Natl. Acad. Sci. U.S.A.* **2015**, *112*, 15384−15389.
(37) Xue, C.; Ye, C.; Zhang, Y.; Ma, Z.; Liu, P.; Zhang, C.; Zhao, X.; Liu, J.; Mu, Y. Development and Application of a Twin Open-Top Chambers Method to Measure Soil HONO Emission in the North China Plain. *Sci. Total Environ.* **2019**, *659*, 621−631.
(38) Yang, W.; Yuan, H.; Han, C.; Yang, H.; Xue, X. Photochemical Emissions of HONO, NO_2 and NO from the Soil Surface under Simulated Sunlight. *Atmos. Environ.* **2020**, *234*, 117596.
(39) Meusel, H.; Tamm, A.; Kuhn, U.; Wu, D.; Leifke, A. L.; Fiedler, S.; Ruckteschler, N.; Yordanova, P.; Lang-Yona, N.; Pöhlker, M.; Lelieveld, J.; Hoffmann, T.; Pöschl, U.; Su, H.; Weber, B.; Cheng, Y.; Leifke, A. L.; Fiedler, S.; Ruckteschler, N.; Yordanova, P.; Lang-Yona, N.; Pöhlker, M.; Lelieveld, J.; Hoffmann, T.; Pöschl, U.; Su, H.; Weber, B.; Cheng, Y. Emission of Nitrous Acid from Soil and Biological Soil Crusts Represents an Important Source of HONO in the Remote Atmosphere in Cyprus. *Atmos. Chem. Phys.* **2018**, *18*, 799−813.
(40) Wu, D.; Horn, M. A.; Behrendt, T.; Müller, S.; Li, J.; Cole, J. A.; Xie, B.; Ju, X.; Li, G.; Ermel, M.; Oswald, R.; Fröhlich-Nowoisky, J.; Hoor, P.; Hu, C.; Liu, M.; Andreae, M. O.; Pöschl, U.; Cheng, Y.; Su, H.; Trebs, I.; Weber, B.; Sörgel, M. Soil HONO Emissions at High Moisture Content Are Driven by Microbial Nitrate Reduction to Nitrite: Tackling the HONO Puzzle. *ISME J.* **2019**, *13*, 1688−1699.
(41) Bhattarai, H. R.; Virkajärvi, P.; Yli-Pirilä, P.; Maljanen, M. Emissions of Atmospherically Important Nitrous Acid (HONO) Gas from Northern Grassland Soil Increases in the Presence of Nitrite (NO_2^-). *Agric., Ecosyst. Environ.* **2018**, *256*, 194−199.
(42) Scharko, N. K.; Schütte, U. M. E.; Berke, A. E.; Banina, L.; Peel, H. R.; Donaldson, M. A.; Hemmerich, C.; White, J. R.; Raff, J. D. Combined Flux Chamber and Genomics Approach Links Nitrous Acid Emissions to Ammonia Oxidizing Bacteria and Archaea in Urban and Agricultural Soil. *Environ. Sci. Technol.* **2015**, *49*, 13825−13834.
(43) Xue, C.; Ye, C.; Zhang, C.; Catoire, V.; Liu, P.; Gu, R.; Zhang, J.; Ma, Z.; Zhao, X.; Zhang, W.; Ren, Y.; Krysztofiak, G.; Tong, S.; Xue, L.; An, J.; Ge, M.; Mellouki, A.; Mu, Y. Evidence for Strong HONO Emission from Fertilized Agricultural Fields and Its Remarkable Impact on Regional O_3 Pollution in the Summer North China Plain. *ACS Earth Space Chem.* **2021**, *5*, 340−347.
(44) Laufs, S.; Cazaunau, M.; Stella, P.; Kurtenbach, R.; Cellier, P.; Mellouki, A.; Loubet, B.; Kleffmann, J. Diurnal Fluxes of HONO above a Crop Rotation. *Atmos. Chem. Phys.* **2017**, *17*, 6907−6923.
(45) Ren, X.; Sanders, J. E.; Rajendran, A.; Weber, R. J.; Goldstein, A. H.; Pusede, S. E.; Browne, E. C.; Min, K.-E.; Cohen, R. C. A Relaxed Eddy Accumulation System for Measuring Vertical Fluxes of Nitrous Acid. *Atmos. Meas. Tech.* **2011**, *4*, 2093−2103.
(46) Rasool, Q. Z.; Bash, J. O.; Cohan, D. S. Mechanistic Representation of Soil Nitrogen Emissions in the Community Multiscale Air Quality (CMAQ) Model v 5.1. *Geosci. Model Dev.* **2019**, *12*, 849−878.
(47) Porada, P.; Tamm, A.; Raggio, J.; Cheng, Y.; Kleidon, A.; Pöschl, U.; Weber, B. Global NO and HONO Emissions of Biological Soil Crusts Estimated by a Process-Based Non-Vascular Vegetation Model. *Biogeosciences* **2019**, *16*, 2003−2031.
(48) Kim, M.; Or, D. Microscale PH Variations during Drying of Soils and Desert Biocrusts Affect HONO and NH3 Emissions. *Nat. Commun.* **2019**, *10*, 3944.
(49) Kim, M.; Or, D. Hydration Status and Diurnal Trophic Interactions Shape Microbial Community Function in Desert Biocrusts. *Biogeosciences* **2017**, *14*, 5403−5424.
(50) Su, H.; Chen, C.; Li, M.; Cheng, Y. Estimates of Global Biogenic Soil HONO Emissions Using a Process-Oriented Model. *American Geophysical Union, Fall Meeting*, 2018; pp A33K−A3316.
(51) Wang, Y.; Fu, X.; Wu, D.; Wang, M.; Lu, K.; Mu, Y.; Liu, Z.; Zhang, Y.; Wang, T. Agricultural Fertilization Aggravates Air Pollution by Stimulating Soil Nitrous Acid Emissions at High Soil Moisture. *Environ. Sci. Technol.* **2021**, *55*, 14556.
(52) Sutton, M. A.; Burkhardt, J. K.; Guerin, D.; Nemitz, E.; Fowler, D. Development of Resistance Models to Describe Measurements of Bi-Directional Ammonia Surface−Atmosphere Exchange. *Atmos. Environ.* **1998**, *32*, 473−480.
(53) Trebs, I.; Lara, L. L.; Zeri, L. M. M.; Gatti, L. V.; Artaxo, P.; Dlugi, R.; Slanina, J.; Andreae, M. O.; Meixner, F. X. Dry and Wet Deposition of Inorganic Nitrogen Compounds to a Tropical Pasture Site (Rondônia, Brazil). *Atmos. Chem. Phys.* **2005**, *5*, 3131−3189.

https://doi.org/10.1021/acs.est.1c06716
Environ. Sci. Technol. 2022, 56, 2204−2212

(54) Seinfeld, J. H.; Pandis, S. N. *Atmospheric Chemistry and Physics: From Air Pollution to Climate Change*, 3rd ed.; Wiley: New York, 2016.
(55) Hicks, B. B.; Baldocchi, D. D.; Meyers, T. P.; Hosker, R. P.; Matt, D. R. A Preliminary Multiple Resistance Routine for Deriving Dry Deposition Velocities from Measured Quantities. *Water, Air, Soil Pollut.* **1987**, *36*, 311−330.
(56) Lao, M.; Crilley, L. R.; Salehpoor, L.; Furlani, T. C.; Bourgeois, I.; Neuman, J. A.; Rollins, A. W.; Veres, P. R.; Washenfelder, R. A.; Womack, C. C.; Young, C. J.; Vandenboer, T. C. A Portable, Robust, Stable, and Tunable Calibration Source for Gas-Phase Nitrous Acid (HONO). *Atmos. Meas. Tech.* **2020**, *13*, 5873−5890.
(57) Meusel, H.; Elshorbany, Y.; Kuhn, U.; Bartels-Rausch, T.; Reinmuth-Selzle, K.; Kampf, C. J.; Li, G.; Wang, X.; Lelieveld, J.; Pöschl, U.; Hoffmann, T.; Su, H.; Ammann, M.; Cheng, Y. Light-Induced Protein Nitration and Degradation with HONO Emission. *Atmos. Chem. Phys.* **2017**, *17*, 11819−11833.
(58) Pape, L.; Ammann, C.; Nyfeler-Brunner, A.; Spirig, C.; Hens, K.; Meixner, F. X. An Automated Dynamic Chamber System for Surface Exchange Measurement of Non-Reactive and Reactive Trace Gases of Grassland Ecosystems. *Biogeosciences* **2009**, *6*, 405−429.
(59) VandenBoer, T. C.; Young, C. J.; Talukdar, R. K.; Markovic, M. Z.; Brown, S. S.; Roberts, J. M.; Murphy, J. G. Nocturnal Loss and Daytime Source of Nitrous Acid through Reactive Uptake and Displacement. *Nat. Geosci.* **2015**, *8*, 55−60.
(60) Bohn, H. L.; McNeal, B. L.; O'Connor, G. A. *Soil Chemistry*, 2nd ed.; Academic Press, 2001.
(61) Donaldson, M. A.; Berke, A. E.; Raff, J. D. Uptake of Gas Phase Nitrous Acid onto Boundary Layer Soil Surfaces. *Environ. Sci. Technol.* **2014**, *48*, 375−383.
(62) Harrison, R. M.; Peak, J. D.; Collins, G. M. Tropospheric Cycle of Nitrous Acid. *J. Geophys. Res.: Atmos.* **1996**, *101*, 14429−14439.
(63) Harrison, R. M.; Kitto, A.-M. N. Evidence for a Surface Source of Atmospheric Nitrous Acid. *Atmos. Environ.* **1994**, *28*, 1089−1094.
(64) Li, X.; Brauers, T.; Häseler, R.; Bohn, B.; Fuchs, H.; Hofzumahaus, A.; Holland, F.; Lou, S.; Lu, K. D.; Rohrer, F.; Hu, M.; Zeng, L. M.; Zhang, Y. H.; Garland, R. M.; Su, H.; Nowak, A.; Wiedensohler, A.; Takegawa, N.; Shao, M.; Wahner, A. Exploring the Atmospheric Chemistry of Nitrous Acid (HONO) at a Rural Site in Southern China. *Atmos. Chem. Phys.* **2012**, *12*, 1497−1513.
(65) Stutz, J.; Alicke, B.; Neftel, A. Nitrous acid formation in the urban atmosphere: Gradient measurements of NO2and HONO over grass in Milan, Italy. *J. Geophys. Res.: Atmos.* **2002**, *107*, 5.
(66) Tang, K.; Qin, M.; Duan, J.; Fang, W.; Meng, F.; Liang, S.; Xie, P.; Liu, J.; Liu, W.; Xue, C.; Mu, Y. A Dual Dynamic Chamber System Based on IBBCEAS for Measuring Fluxes of Nitrous Acid in Agricultural Fields in the North China Plain. *Atmos. Environ.* **2019**, *196*, 10−19.
(67) Maier, S.; Kratz, A. M.; Weber, J.; Prass, M.; Liu, F.; Clark, A. T.; Abed, R. M. M.; Su, H.; Cheng, Y.; Eickhorst, T.; Fiedler, S.; Pöschl, U.; Weber, B. Water-Driven Microbial Nitrogen Transformations in Biological Soil Crusts Causing Atmospheric Nitrous Acid and Nitric Oxide Emissions. *ISME J.* **2021**, *2021*, 1−13.
(68) Zhang, W.; Tong, S.; Jia, C.; Wang, L.; Liu, B.; Tang, G.; Ji, D.; Hu, B.; Liu, Z.; Li, W.; Wang, Z.; Liu, Y.; Wang, Y.; Ge, M. Different HONO Sources for Three Layers at the Urban Area of Beijing. *Environ. Sci. Technol.* **2020**, *54*, 12870.

https://doi.org/10.1021/acs.est.1c06716
Environ. Sci. Technol. 2022, 56, 2204−2212